



Semiconductorlike photocarrier dynamics in Dirac-semimetal Cd_3As_2 films probed with transient terahertz spectroscopy

Wenjie Zhang,¹ Yunkun Yang,² Peng Suo,¹ Kaiwen Sun,¹ Jun Peng,¹ Xian Lin ,¹ Faxian Xiu,² and Guohong Ma ^{1,*}

¹*Department of Physics, Shanghai University, Shanghai 200444, China*

²*State Key Laboratory of Surface Physics and Department of Physics, Fudan University, Shanghai 200433, China*



(Received 16 June 2022; revised 31 July 2022; accepted 7 October 2022; published 20 October 2022)

The topological three-dimensional Dirac semimetal Cd_3As_2 has drawn great attention for the novel physics and promising applications in optoelectronic devices operating in the infrared and terahertz (THz) regimes. Among the extensive studies in the past decades, one intriguing debate is the underlined mechanism governing the nonequilibrium carrier dynamics following photoexcitation. In this study, the temperature-dependent photocarrier dynamics in Cd_3As_2 film has been investigated with time-resolved terahertz spectroscopy. The experimental results demonstrate that photoexcitation results in abrupt increase in THz photoconductivity, and the subsequent relaxation shows a single exponential relaxation for various temperatures and pump fluences. The relaxation time increases from 4.7 ps at 5 K to 7.5 ps at 220 K, while the lifetime remains almost constant at ~ 7.5 ps with temperature above 220 K. A Rothwarf-Taylor model was employed to fit the temperature-dependent relaxation time, and a narrow energy gap of $\sim 35 \pm 6$ meV is obtained, which occurs around the Dirac node. Our THz spectroscopy results demonstrate that the photocarrier relaxation in Cd_3As_2 shows a semiconductorlike behavior, rather than hot-carrier scatterings in graphene and most of metals.

DOI: [10.1103/PhysRevB.106.155137](https://doi.org/10.1103/PhysRevB.106.155137)

I. INTRODUCTION

Three-dimensional (3D) Dirac semimetals (DSMs), with their gapless feature and linear energy dispersion in the energy-momentum diagram, have attracted enormous interest as a new family of topological quantum materials [1–5]. Owing to the massless Fermion energy dispersion, DSMs usually have high carrier mobility and a tunable chemical potential, resulting in potential applications in electronics and optoelectronics [6–10]. Conventionally, DSMs have a large absorption coefficient and ultrafast response in the infrared and terahertz (THz) region [11–13], and thus show appealing application in designing the advanced optoelectronic devices for far-infrared radiation. As a member of 3D DSMs, Cd_3As_2 has been paid considerable attention due to its high stability and large linear energy-momentum space. In the past decades, massive studies have been carried out for exploring the equilibrium transportation in Cd_3As_2 , which revealed that the DSM Cd_3As_2 shows high carrier mobility [14–16], large magnetoresistance [17–19], magneto-optical response [20], and the nonlinear optical response in the THz regime [21,22]. To gain more practical applications, understanding the nonequilibrium carrier dynamics in Cd_3As_2 is important for developing high-speed and broadband photodetectors or modulators benefiting from its high carrier mobility and conical Dirac bands [23,24].

Although many studies have been carried out on the photocarrier dynamics in Cd_3As_2 through various probe methods, such as photocurrent [23], transient infrared reflection [25–28], transient THz spectroscopy [29–32], time-resolved

angle-resolved photoemission spectroscopy [33], and high harmonic generation [34], the underlined mechanism governing the photocarrier dynamics of Cd_3As_2 is still under debate. In general, two different models are proposed to discuss the photocarrier dynamics in Cd_3As_2 with photoexcitation depending on the intra- and interband scattering rate [35]. If the interband scattering is faster than that of intraband scattering, the resultant quasiequilibrium can be described by a Fermi-Dirac distribution. Carrier-phonon coupling leads to the cooling of hot carriers, and photocarrier dynamics can be interpreted with the two-temperature model (TTM) [27,29,36]; this model has been widely accounted for the photocarrier dynamics in metals [36–38]. On the other hand, if the intraband scattering is much faster than that of interband scattering/recombination, the photoexcited electrons and holes could establish the separated Fermi distribution with electrons in conduction band and holes in valence band, respectively [32], especially when high symmetry of the ideal system is broken, and a band gap opens at the Dirac point [26]. This picture is similar to semiconductor materials, in which the Rothwarf-Taylor (RT) model is applicable [35].

Terahertz radiation has very low photon energy of a few meV, which makes the THz spectroscopy a sensitive tool for measuring the conductivity change of the free carrier; it is especially useful to probe the ultrafast photoconductivity (PC) around the Fermi surface of materials. In this work, we utilize the time-resolved THz spectroscopy to investigate photocarrier dynamics of a 50-nm Cd_3As_2 film with various pump fluence and temperature. Our experimental results demonstrate that an optical pump of 780 nm leads to the sharp increase in THz-positive PC in Cd_3As_2 film; the subsequent relaxation of PC follows a single exponential decay.

*ghma@staff.shu.edu.cn

Interestingly, the decaying time τ of PC shows a complex temperature dependence, which increases from 4.7 ps at 5 K to 7.5 ps at 220 K, while the magnitude of τ remains almost constant when the temperature is above 220 K. Additionally, it is also noted that the pump-fluence dependence of the decaying time τ varies greatly at different temperatures, in which τ increases with pump fluence at low temperature, while it remains constant at room temperature. Meanwhile, the THz PC dispersion obtained at various temperatures, pump fluences, and delay times can be well fitted with the Drude model. These THz experimental results reveal that the increase in THz PC after photoexcitation mainly arises from the increase in carrier population, and the subsequent relaxation is dominated by the electron-hole (e-h) recombination, which suggests that photocarrier dynamics in Cd₃As₂ shows a semiconductorlike behavior, and the RT model is employed to fit the temperature-dependent THz relaxation time. The fitting results indicate that a narrow band gap with magnitude of 35 ± 6 meV exists at the Dirac points for the 50-nm Cd₃As₂ thin film. The coexistence of the high-frequency phonons (HFPs) generation and e-h recombination results in a phonon bottleneck effect, which slows down the photocarrier dynamics at high temperature. Our THz spectroscopy results demonstrate that the photocarrier relaxation in Cd₃As₂ shows a semiconductorlike behavior, rather than hot-carrier scatterings in graphene and most metals.

II. METHODS

Optical pump and terahertz probe (OPTP) experiments in the transmission configuration were performed to explore the dynamics of photocarriers in Cd₃As₂ thin film. The optical pulses are delivered from a Ti:sapphire amplifier with 120-femtoseconds (fs) duration at central wavelength of 780 nm (1.59 eV) and a repetition rate of 1 kHz. The THz emitter and detector are based on a pair of (110)-oriented ZnTe crystals. The optical pump and THz probe pulse are collinearly polarized with a spot size of 6.5 and 2.0 mm on the surface of sample, respectively. All measurements were conducted in a dry nitrogen atmosphere, and the samples were placed in a cryostat with temperature varying from 5 to 300 K.

III. EXPERIMENTAL RESULTS

The high-quality Cd₃As₂ film was grown via a molecular-beam epitaxy system on sapphire substrate. Before growing the Cd₃As₂ film, a 10-nm-thick CdTe buffer layer was deposited to assist the Cd₃As₂ nucleation. The Cd₃As₂ film was grown epitaxially onto the buffer layer at 100°C, and the thickness is approximately 50 nm. The Fermi level of the intrinsic film is about 210 meV [32]. Figure 1(a) shows the x-ray-diffraction pattern of the Cd₃As₂ film. The sharp diffraction peak located around $2\theta = 24.3^\circ$ is indexed as (224) [39]. A shoulder peak at the left side of (224) is contributed by the (111) index of buffer layer CdTe. It is clear that the full width at half maximum of the (224) peak is less than 0.18° , verifying the high crystallinity of the Cd₃As₂ thin film. Figure 1(b) shows the temperature-dependent carrier density measured by the Hall effect. It is seen that the carrier

concentration increases slightly from $n \approx 9.95 \times 10^{17} \text{ cm}^{-3}$ at 5 K to $1.07 \times 10^{18} \text{ cm}^{-3}$ at room temperature. The Raman scattering under 532-nm excitation along with Gaussian fitting are shown in Fig. 1(c); four pronounced peaks located around 62.2 (B_{1g}), 139.5 (A_{1g}), 174.3 (B_{1g}), and 194.5 cm^{-1} (B_{1g}) are consistent with the previous reports in the literature [40,41], suggesting centrosymmetric structure for our 50-nm-thick Cd₃As₂ film.

Figure 1(d) shows the transmitted THz waveform through the film without pump (blue) and differential transmitted THz waveform with pump beam at $\Delta t = 0$ ps (red), respectively. The photoinduced change in the THz electric field is expressed as $\Delta E(t, \Delta t) = E(t, \Delta t) - E_{\text{ref}}(t)$, where $E(t, \Delta t)$ and $E_{\text{ref}}(t)$ are the time-domain THz waveform at Δt with and without pump, respectively, and t is the electro-optical sampling delay time for the distinction from the pump-probe delay time Δt . It is clear that THz-transmitted waveforms collected at $\Delta t = 0$ ps show out of phase with that of $E_{\text{ref}}(t)$, indicating the pump pulse induced the reduction of the THz transmission (increase of THz PC). By varying the delay time between the 780-nm optical- and the THz pulses, the transient THz transmission can be mapped out through measuring the photoinduced peak absorption. The inset of Fig. 1(d) plots the THz peak modulation $M = |(T(\Delta t = 0) - T_0)/T_0|$ with respect to pump fluence at room temperature, in which $T(\Delta t = 0)$ and T_0 stand for the THz peak transmission at zero delay time with pump and without pump, respectively. The THz peak transmission shows linear dependence of pump fluence in both low- and high-pump fluence regimes: in a low-fluence regime of $F < 25 \mu\text{J}/\text{cm}^2$, the THz modulation depth is less than 15% with a linear slope of 2.46 mJ^{-1} , while in a high-fluence regime of $F > 0.1 \text{ mJ}/\text{cm}^2$ regime, the THz modulation depth is higher than 50% with slope of 0.16 mJ^{-1} . Transient THz PC response under high pump fluence ($F > 0.1 \text{ mJ}/\text{cm}^2$) had been studied in our previous work [32]. Here, we mainly focused our study on the low pump-fluence regime with $F \leq 25 \mu\text{J}/\text{cm}^2$.

Figures 2(a) and 2(c) show the transient THz transmission, $\Delta T/T_0$, at 5 K with three selective pump fluences of 6.25, 18.75, and $25 \mu\text{J}/\text{cm}^2$ [Fig. 2(a)] as well as $\Delta T/T_0$ with fixed pump fluence of $18.75 \mu\text{J}/\text{cm}^2$ for three selective temperatures of 20, 140, and 300 K [Fig. 2(c)]. The small kink appearing around 17 ps in Figs. 2(a) and 2(c) comes from secondary reflection of optical pulse on the 1-mm ZnTe, the THz emitter, which is negligible during exponential fitting. It is clear that the photoexcitation leads to the abrupt decrease in THz transmission, indicating the increase in THz photoconductivity for all measured temperatures and pump fluences. The transient THz trace can be well reproduced with single exponential function,

$$\frac{\Delta T}{T_0}(t) = A \cdot e^{\omega^2/\tau^2 - t/\tau} \cdot \text{erfc}\left(\frac{2\omega}{\tau} - \frac{t}{2\omega}\right) + B, \quad (1)$$

in which τ , A , and B are the decay lifetime, amplitude, and offset, respectively; $2\omega = 0.4$ ps is the THz pulse width, and $\text{erfc}(t) = 1 - \text{erf}(t)$ is a complementary error function. The best fittings are also presented with solid lines. The positive THz PC following photoexcitation suggests that the increase in the Drude weight is larger than the increase in scattering

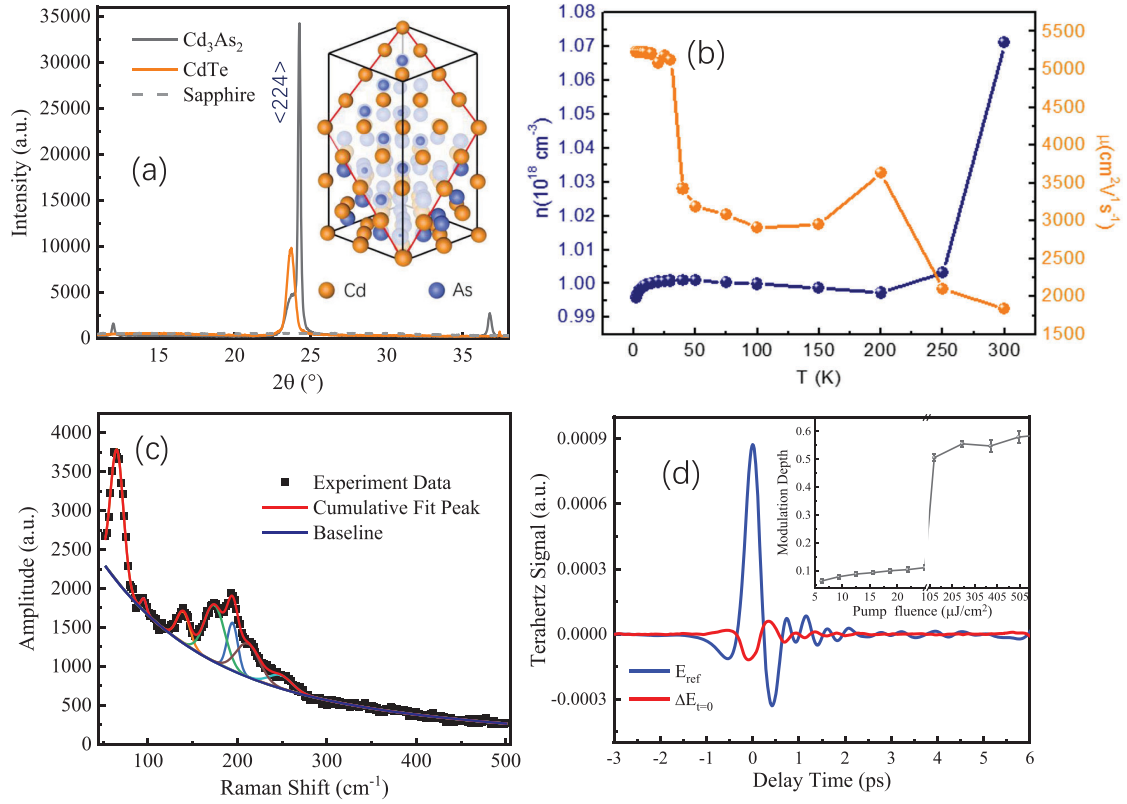


FIG. 1. (a) X-ray diffraction patterns of Cd_3As_2 film; the peak around $2\theta = 24.3^\circ$ corresponds to (224) diffraction. Inset illustrates the crystal structure of Cd_3As_2 along (112) plane. (b) Temperature-dependent carrier density and mobility of the 50-nm Cd_3As_2 film. (c) Raman spectroscopy of Cd_3As_2 film along with Gaussian fittings. (d) THz waveform transmission of the sample without pump (blue) and THz differential waveform with pump fluence of $18.75 \mu\text{J}/\text{cm}^2$ at delay time $\Delta t = 0$ ps (red), respectively. Inset shows the THz modulation with respect to pump fluence at room temperature.

rate with photoexcitation. The increase in Drude weight could be contributed by the elevated electron temperature and/or increase in carrier population. Due to the constraint of linear dispersion band structure in Cd_3As_2 semimetal, it could be possible that the increase in Drude weight is larger than that in the scattering rate at elevated electron temperature caused by optical injection [42,43], so that the free carriers' absorption of THz radiation is enhanced by hot electrons due to the intraband transition undergoing larger possible momentum- and energy-conservation spaces. Considering very large electron capacity ($\gamma_e \approx 70 \text{ J K}^{-2} \text{ m}^{-3}$) in Cd_3As_2 [33,35], the increase in THz PC due to the elevated electron temperature is calculated to be less than 1% under pump fluence of $25 \mu\text{J}/\text{cm}^2$, as shown in Sec. 1 of Supplemental Material [44]. While the increase in THz PC is above 10%, which can be seen clearly from Figs. 2(a) and 2(c), therefore it is reasonable to assign the positive THz PC observed in Figs. 2(a) and 2(c) to the increase of carrier population following photoexcitation.

In order to further verify the THz PC is contributed by the increase of photocarrier density (ΔN) rather than increase in carrier temperature, we have also measured the PC at different pump fluence, delay time, and temperatures, and the experimental results are displayed in Figs. 2(b), 2(d), 2(e), and 2(f), respectively. For the 50-nm film of Cd_3As_2 , the Tinkham equation is applicable, in which transient THz transmission,

time-dependent $\Delta T/T_0$ can be transformed into complex PC in frequency region. According to the thin-film approximation, the real ($\Delta\sigma_r$) and imaginary ($\Delta\sigma_i$) PC is given by [32,45]

$$\Delta\sigma_r = \left(\frac{\cos \phi}{E} - 1 \right) \frac{1 + n_{\text{sub}}}{Z_0}, \quad (2a)$$

$$\Delta\sigma_i = - \frac{(1 + n_{\text{sub}}) \sin \phi}{EZ_0}, \quad (2b)$$

where E is the amplitude ratio of the Fourier-transformed THz signal for unexcited sample and excited sample, and ϕ is the phase difference of these two; n_{sub} and Z_0 are refractive index of substrate with $n_{\text{sub}} = 3$ and free-space impedance with $Z_0 \approx 377 \Omega$, respectively. Figures 2(b) and 2(d) present the real and imaginary PC dispersion measured at 5 K with various pump fluences [Fig. 2(b)], and different temperature with fixed fluence of $18.75 \mu\text{J}/\text{cm}^2$ [Fig. 2(d)]; both of them are measured at delay time of 1 ps. The solid lines are the best fitting with the Drude model:

$$\Delta\tilde{\sigma} = \frac{\varepsilon_0 \omega_p^2 \tau_k}{1 - i\omega\tau_k} = \frac{\Delta\sigma_{dc}}{1 - i\omega\tau_k}, \quad (3)$$

in which ε_0 , ω_p , and τ_k are the vacuum permittivity, plasma frequency, and scattering time, respectively. It is clear from

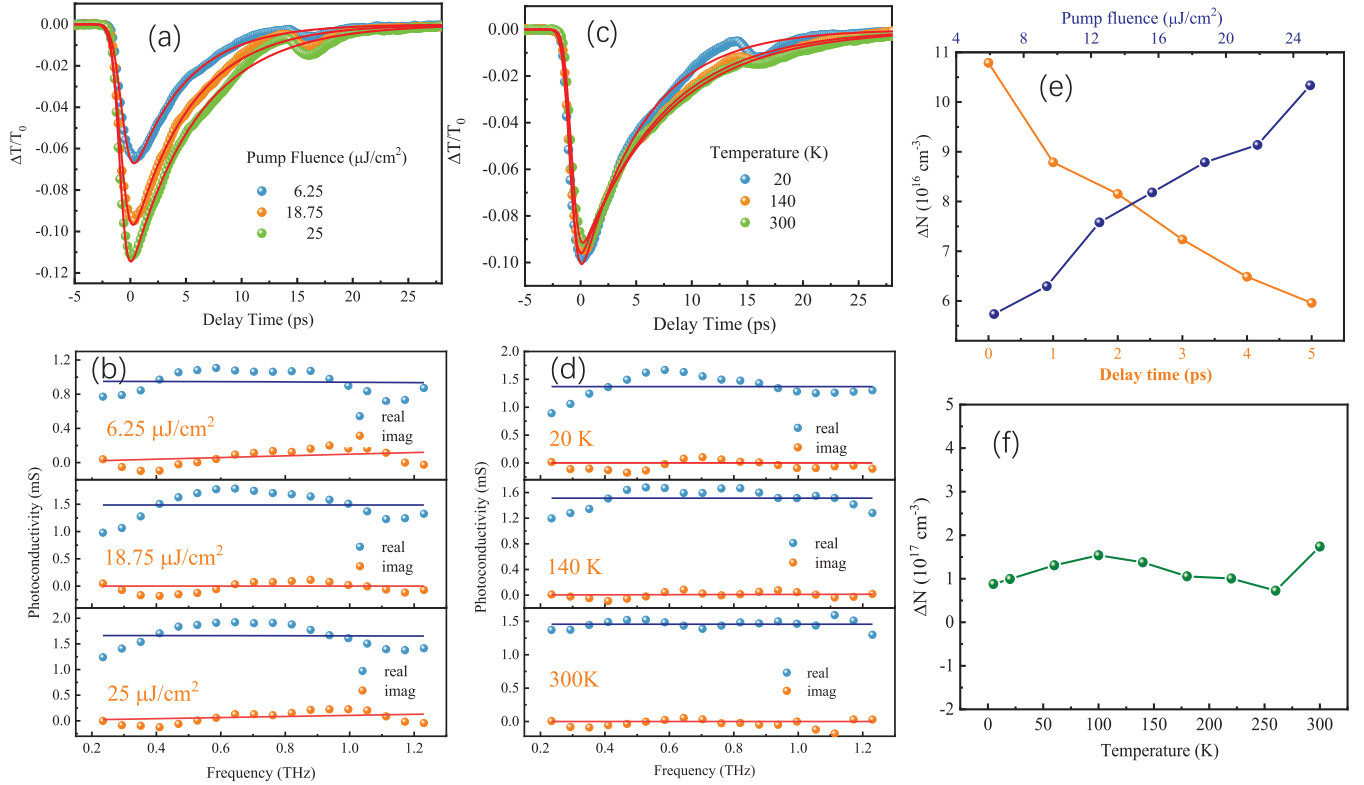


FIG. 2. (a) Transient THz transmission under pump fluence of 6.25, 18.75, and 25 $\mu\text{J}/\text{cm}^2$ at 5 K along with single exponential fitting (solid lines), (b) corresponding PC dispersion measured at delay time $\Delta t = 0$ in (a), with the solid lines of Drude model fitting. (c) Transient THz transmission at temperature of 20, 140, and 300 K under pump fluence of 18.75 $\mu\text{J}/\text{cm}^2$, along with single exponential fitting (solid lines), (d) corresponding PC dispersion obtained at delay time $\Delta t = 0$ in (c), with the solid lines of Drude model fitting. (e) Fitting carrier concentration change (ΔN) with respect to pump fluence and delay time at 5 K. (f) Fitting carrier concentration change (ΔN) with respect to temperature obtained at delay time of 1 ps and pump fluence of 18.75 $\mu\text{J}/\text{cm}^2$.

Figs. 2(b) and 2(d) that the fitting curves with the Drude model deviate from the experimental data, and the deviations become more pronounced at lower temperature. This departure is mainly due to the existence of optical phonon mode around 0.6 THz for Cd_3As_2 that has been reported in previous study [31]. Figure 2(e) presents the photocarrier density $\Delta N = \frac{\omega_p^2 \epsilon_0 \tau_k}{e^2}$ with respect to pump fluence (blue) and delay time (orange), respectively. It is seen that ΔN increases with pump fluence and decreases with delay time, indicating photoexcitation does increase the carrier population, and the decay of photocarrier occurs via depopulation of carriers, probable via e-h recombination instead of hot carrier cooling. In addition, Fig. 2(f) presents the photocarrier density with respect to temperature; it is clearly seen that the photocarrier density almost does not change with temperature. The fitting-momentum scattering time, τ_k , with respect to pump fluence, delay time, and temperature, is given in Sec. 2 of Supplemental Material [44], which shows good agreement with the prediction that photoexcitation induced the increase of carrier population.

IV. DISCUSSIONS

In Ref. [30], the authors ascribed the positive THz PC in Cd_3As_2 film to the elevated temperature of carriers around the

Fermi surface following optical excitation, and the subsequent relaxation was interpreted as the electrons' cooling process, in which TTM was applied to model the relaxation process. Our THz experimental data along with Drude fitting presented in Fig. 2 demonstrated that an increase of carrier population plays a dominate role in the positive THz PC, while the hot-carrier contribution is one order of magnitude less than that of the increase in carrier population. We propose that photoexcitation of Cd_3As_2 film results in the increase in both carrier temperature and carrier density, but the latter plays a more pronounced role in the positive THz PC; as a result, the photoresponse of Cd_3As_2 film shows semiconductorlike behavior. After photoexcitation, subsequent relaxation in Cd_3As_2 film behaves with both temperature- and pump-fluence dependence, which can be well reproduced with single exponential decay function. The relaxation process is then proposed to be dominated by the photocarrier depopulation via e-h recombination in Cd_3As_2 following optical excitation. In the following part, we will discuss the possible originality of the photocarrier relaxation in Cd_3As_2 film. Figure 3(a) presents the fitting-time constants versus pump fluence at 5 and 300 K, respectively. It is obvious that at low temperature of 5 K, the decay time slows down from 4.7 to 6.1 ps as the pump fluence increases from 6.25 to 25 $\mu\text{J}/\text{cm}^2$, while this change was not observed at room temperature, in which the life-

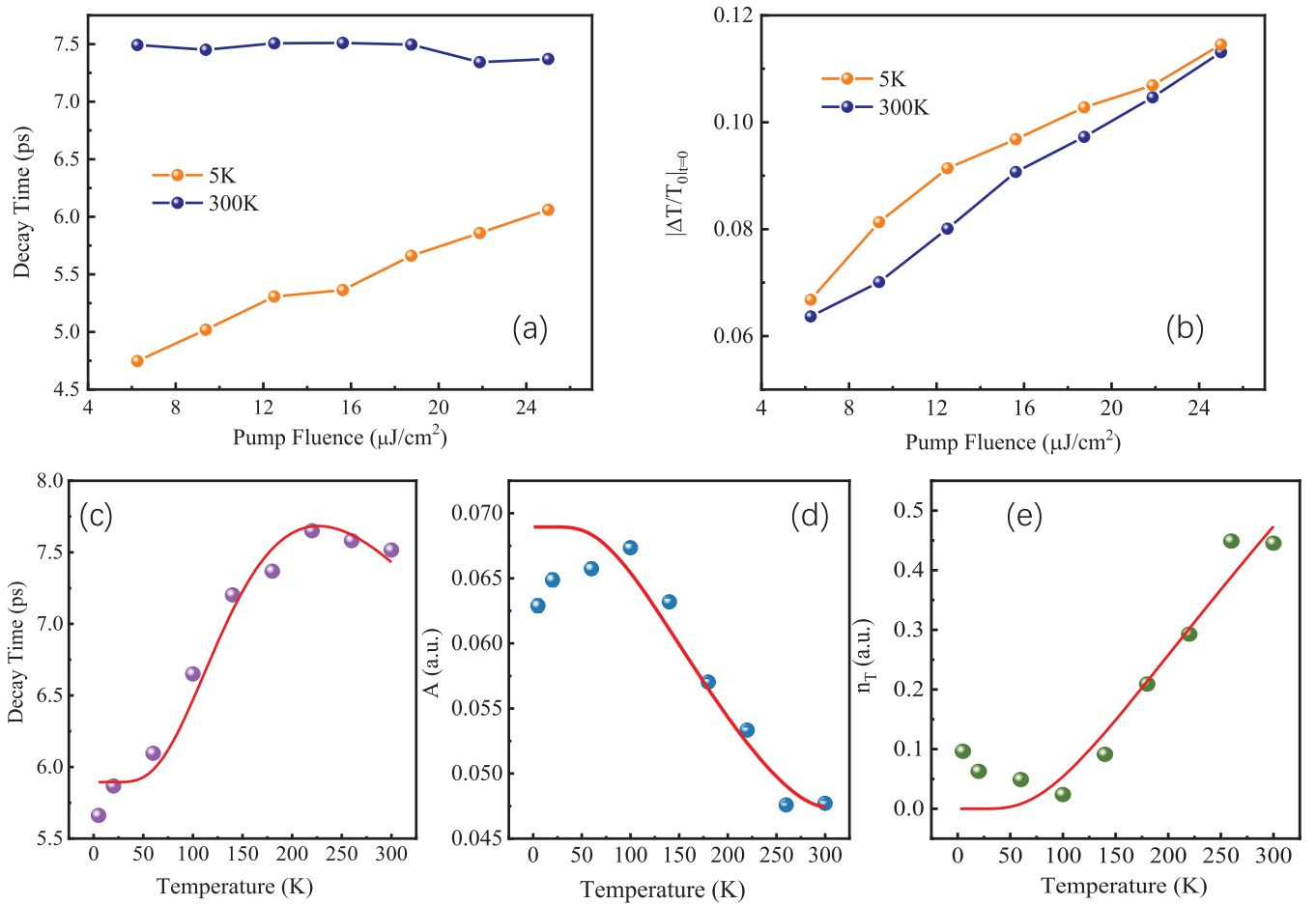


FIG. 3. (a) Relaxation time τ obtained from single exponential fitting [Eq. (1)] with respect to pump fluence at 5 K (orange dots) and 300 K (blue dots). (b) $|\Delta T/T_0|_{t=0}$ of the transient THz signal with different pump fluence at 5 K and room temperature. (c) Temperature-dependent relaxation time τ (purple dots); red line is the fitting curve with RT model. (d) Temperature-dependent amplitude A (blue dots); red line is the fitting curve with RT model. (e) Thermally populated carrier density per unit cell n_T vs temperature calculated by RT model.

time remains 7.5 ps with various pump fluences. Figure 3(b) presents the fitting lifetime with respect to temperatures under pump fluence of $18.75 \mu\text{J}/\text{cm}^2$. Interestingly, it is noted that when the temperature is lower than 220 K, the relaxation time increases with temperature under identical pump fluence, and the relaxation time remains unchanged when the temperature is higher than 220 K.

The pump-fluence dependence at room temperature [Fig. 3(a)] and temperature dependence of relaxation time [Fig. 3(c)] for our Cd_3As_2 thin film cannot be interpreted with the TTM. According to the TTM, the electron-electron (e-e) thermalization is much faster than electron-phonon (e-ph) thermalization after photoexcitation, and the electrons with the elevated temperature transfer the excess energy to lattice via e-ph coupling until the two subsystems reach a balanced temperature. Therefore, the hot carrier relaxation time is expected to be longer as the pump fluence increases, which cannot interpret our experimental finding in Fig. 3(a). It should be noted that Fig. 3(b) shows the $|\Delta T/T_0|_{t=0}$ increase with the pump fluence, while the relaxation lifetime remains constant at room temperature, which suggests that the fluence we use is not saturated. Furthermore, the carrier lifetime remaining unchanged for temperature above 220 K is also beyond the TTM. It is noted that the e-ph coupling time is

conventionally less than 2 ps in most metal and semimetal materials, which is threefold faster than the relaxation time in our Cd_3As_2 film. This anomalous pump fluence and temperature dependence of relaxation time in the Cd_3As_2 film suggests a different underlying mechanism dominates the photocarrier relaxation. It is noted that Cd_3As_2 will undergo semimetal to semiconductor transition with decreasing the film thickness [46], and gap opening in a Cd_3As_2 thin film has been predicted theoretically [1] and verified experimentally [47]. Our previous study also indicated the semiconductorlike character for the photocarrier relaxation in Cd_3As_2 films [32]. Therefore, it is reasonable to assume that our 50-nm thick film is thin enough to open a narrow gap at the Dirac point, which will have a profound effect on the photocarrier dynamics following optical excitation. It has been demonstrated that the RT model is applicable to analyze the nonequilibrium carrier dynamics in narrow-gap structure, such as superconductor gap [48,49], charge-density wave gap [50], as well as collective hybridization [51].

Here, we employ the RT model to fit the temperature-dependent relaxation time. The RT model was originally proposed to address the ultrafast relaxation mechanism in superconductivity [52]. Later, it was shown to be suitable for a variety of materials with gap openings in the density

of states [53,54]. In these systems, photoexcitation produces large numbers of quasiparticles (QPs) that decay towards an initial equilibrium state through e-e or e-ph interactions. In the RT model, the formation of an energy gap would introduce a phonon bottleneck effect, which would significantly impede the relaxation of QPs. The source of the phonon bottleneck effect is that HFPs are generated when QPs recombine across the energy gap, which may in turn induce the excitation of a large number of QPs, thereby prolonging the relaxation time of the entire system. Based on this model, the density of thermally activated QPs n_T can be obtained via the amplitude $A(T)$ [55,56],

$$n_T = \frac{\eta}{4R} \left[\frac{A(0)}{A(T)} - 1 \right], \quad (4)$$

where η is the e-h pair regeneration rate due to annihilation of HFPs, R is the recombination rate of e-h pairs, $A(T)$ is the temperature-dependent decay amplitude of the QPs' dynamics, which we obtained by the single exponential fitting of transient THz transmission. The value of $A(0) = 0.068$ is determined by extrapolating the $A(T)$ curve from $T > 100$ K to room temperature [Fig. 3(d), solid line]. The blue dots in Fig. 3(d) are the fitting parameter $A(T)$ with respect to temperature. Moreover, in the RT model, the decay rate of pump-probe dynamics could be described as [57]

$$\tau^{-1} = \Gamma[\delta(n_T + 1)^{-1} + 2n_T], \quad (5)$$

where $\Gamma = \frac{2R\gamma}{\eta^2(1+2\gamma/\eta)}$, R and η are defined above, and γ is the decay rate of HFPs. The coefficient Γ relates the QPs' density and the constant δ relates the photoexcited carrier density to the decay rate; both of them are independent of temperature. n_T is given by the RT model, which takes a general form [52,55]:

$$n_T \propto T^{0.5} \exp\left(-\frac{\Delta}{2k_B T}\right), \quad (6)$$

where Δ is the gap energy. By fitting the temperature-dependent decay time [Fig. 3(c)] and amplitude [Fig. 3(d)] simultaneously with the equations above, we obtain the temperature-dependent n_T as shown in Fig. 3(e), and the gap energy of $\Delta = 35 \pm 6$ meV, which is consistent with the band-gap width induced by symmetry breaking such as doping [20], reducing the dimension [47], or introducing Cd as antisite defects [58]. The deviations at temperature lower than 100 K in Figs. 3(c) and 3(d) may be related to the large increase in mobility at low temperature. The red solid lines in Figs. 3(b), 3(c) and 3(d) present the best fitting of temperature-dependent A , τ , and n_T with the RT model. It is clear that the RT model can fit the experimental data well.

According to the RT model, the increase in temperature results in more HFPs being excited, which slows down the decay process, as we see in Fig. 3(c), with temperature below 220 K. The increase in temperature also produces more thermal carriers n_T , leading to the increases of e-e scattering rate, and the e-h recombination rate could be accelerated assisted by hot carriers; as a result, the temperature-dependent relaxation time is the balanced results between hot-carrier promoted e-h recombination and HFP bottle effect. Taking both the reflection and transmission of the film into account,

the absorbed photon density is $\sim 1.2 \times 10^{17} \text{ cm}^{-3}$ at $18.75 \mu\text{J}/\text{cm}^2$, and the photocarrier density reaches about 10% of the carrier density in equilibrium state. Therefore, the pump-fluence dependent decay time at room temperature hardly changes with the pump fluence, as illustrated with blue dots in Fig. 3(a), where the slight decrease with pump fluence is due to the increase in hot-carrier assisted e-h recombination rate. In contrast, the decay time is seen to increase with pump fluence at 5 K as shown in Fig. 3(a), which is believed to be caused by elevated temperature of the film with photoexcitation. According to the analysis above, photocarrier dynamics in Cd_3As_2 thin film conforms to the RT model, which reveals that the Drude weight increases much more than the scattering rate after photoexcitation, resulting in the reduction of THz transmission. On the other hand, the HFPs are generated across the narrow gap caused by the low dimensionality of Cd_3As_2 film, which can reexcite the recombined carriers, thus contributing a bottleneck effect to the recombination process.

Based on the above analysis, time evolution of the photocarrier is illustrated in Fig. 4. After photoexcitation, electrons are photoexcited into the conduction band well above Fermi level, and holes are left far below the Dirac point as illustrated in Fig. 4(b). Subsequently, the hot electrons reach a quasi-Fermi-Dirac distribution in a very short timescale [34], and holes are relaxed to the top of the valence band, i.e., close to the Dirac point as shown in Fig. 4(c). Electron and hole recombination takes place, in which momentum and energy are conserved. Considering the Fermi level of 210 meV above the Dirac point as well as the highest phonon mode of 220 cm^{-1} in Cd_3As_2 [40], it is impossible to excite the electrons from valence band to conduction band by absorbing a phonon in equilibrium condition. However, the carriers are in a nonequilibrium state after photoexcitation. The subsequent e-h recombination occurs around the Dirac point; during this process, electron and hole can also be repopulated in respective conduction- and valence band via HFPs' excitation simultaneously, which can partially compensate the decrease of electron and hole density due to recombination. In brief, carrier repopulation by absorbing HFPs and carrier depopulation by emitting HFPs via e-h recombination take place simultaneously at certain temperature, which is how the phonon bottleneck takes effect in the gapped Cd_3As_2 thin film in a nonequilibrium state.

A recent theory shows that the Auger recombination is strongly suppressed due to vanishing phase space in three-dimensional materials with linear gapless energy-momentum relation, and the vanished phase space at the Dirac point is predicted to slow down the interband relaxation in 3D Dirac and Weyl semimetal [33,59,60]. But, the vanishing phase space around Dirac point cannot fully interpret the slowing down of relaxation with increasing temperature in our 50-nm Cd_3As_2 film: the interband relaxation time increases with temperature when temperature is below 220 K, while it remains almost unchanged when temperature is in the range of 220 and 300 K. By considering gap opening at the Dirac point, the phonon bottleneck effect can well interpret the observation of temperature-dependent relaxation process. In addition, with decreasing the thickness of Cd_3As_2 film, gap opening around the Dirac point has been reported in Refs. [47,61]; the gap

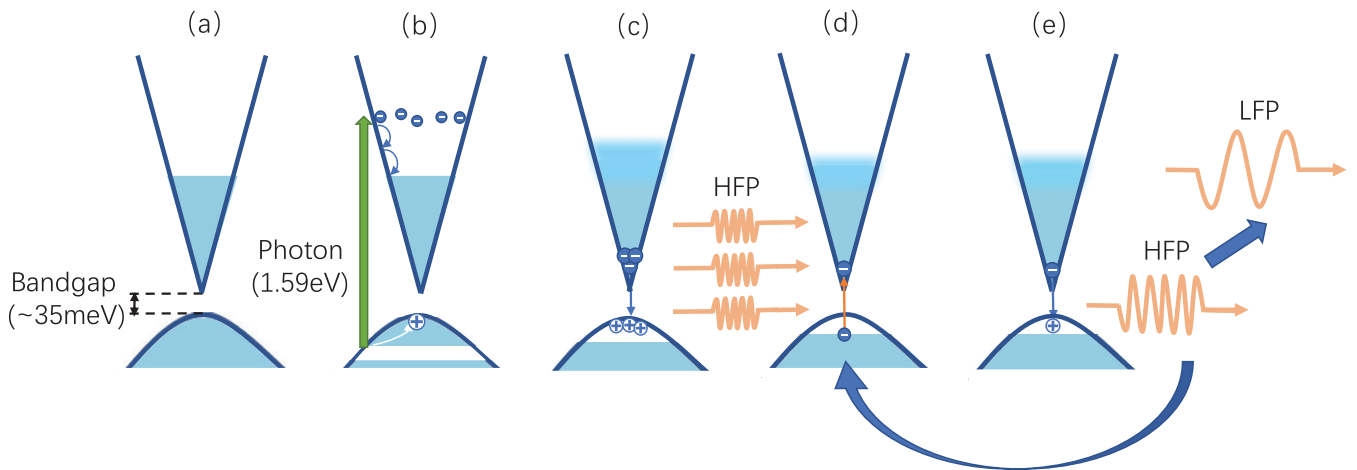


FIG. 4. (a) Before photoexcitation, the Fermi level $E_f = 210$ meV lies above Dirac point of Cd_3As_2 . (b) Generation of electrons and holes by absorption of pump photons of energy 1.59 eV (780 nm). Electrons are promoted into conduction band above Fermi level, and holes are left far below the Dirac point. (c) Holes are relaxed to the top of valence band and combine with the electrons, in which HFPs are generated. (d) Electrons in valence band can be repopulated in conduction band by absorbing HFPs. (e) Recombination of electrons and holes generates new HFPs that induce the phonon bottleneck effect, the HFPs can repopulate the electrons and holes and/or decay into low-frequency phonons (LFPs).

energy of ~ 22 meV was obtained for a 50-nm Cd_3As_2 thin film by measuring temperature-dependent conductivity [61], which is consistent with the result obtained in this study.

V. CONCLUSIONS

To summarize, by employing temperature and pump-fluence dependence of transient THz spectroscopy, we have investigated the photocarrier dynamics in a 50-nm Cd_3As_2 film. Photoexcitation leads to abrupt decrease of THz transmission, and the subsequent relaxation can be well reproduced with single exponential function. The temperature-dependent relaxation time increases with temperature below 220 K, while the relaxation time remains ~ 7.5 ps with temperature above 220 K. The relaxation time shows pump-fluence independence at 300 K, while it increases with pump fluence at low temperature. In addition, our pump fluence, delay time, and temperature dependence of PC dispersion can be well fitted with pure Drude model, which verifies that Drude weight increases more than the scattering rate after photoexcitation, and the relaxation is dominated by depopulating carrier density via e-h recombination. The RT model is employed to

analyze the experimental findings, which demonstrate that gap opening with magnitude of $\Delta = 35 \pm 6$ meV occurs due to the reduced dimensionality in Cd_3As_2 film. The e-h recombination excites HFPs across the narrow gap. In turn, the HFPs can reexcite the carriers, which introduce a phonon bottleneck effect to slow down the carrier dynamics. Moreover, the fitting PC dispersion at various temperatures, pump fluence, and delay times with Drude model clearly demonstrates the applicability of the RT model, and further demonstrates that the photocarrier dynamics in Cd_3As_2 film follows a semiconductorlike behavior. These results are of deep insight into the whole carrier dynamics process in Cd_3As_2 and seeking potential applications in optoelectronics.

ACKNOWLEDGMENTS

This work is supported financially by the National Natural Science Foundation of China (NSFC, Grants No. 92150101 and No. 61735010), and the Science and Technology Commission of Shanghai Municipality (Grant No. 21JC1402600).

The data that support the findings of this study are available from the corresponding authors upon reasonable request.

The authors have no conflicts to disclose.

- [1] Z. Wang, H. Weng, Q. Wu, X. Dai, and Z. Fang, *Phys. Rev. B* **88**, 125427 (2013).
- [2] Z. Wang, Y. Sun, X.-Q. Chen, C. Franchini, G. Xu, H. Weng, X. Dai, and Z. Fang, *Phys. Rev. B* **85**, 195320 (2012).
- [3] Z. K. Liu, B. Zhou, Y. Zhang, Z. J. Wang, H. M. Weng, D. Prabhakaran, S.-K. Mo, Z. X. Shen, Z. Fang, X. Dai, Z. Hussain, and Y. L. Chen, *Science* **343**, 864 (2014).
- [4] T. Zhang, Z. Cui, Z. Wang, H. Weng, and Z. Fang, *Phys. Rev. B* **101**, 115145 (2020).
- [5] K. Nakayama, Z. Wang, D. Takane, S. Souma, Y. Kubota, Y. Nakata, C. Cacho, T. Kim, S. A. Ekahana, M. Shi, M. Kitamura, K. Horiba, H. Kumigashira, T. Takahashi, Y. Ando, and T. Sato, *Phys. Rev. B* **102**, 041104(R) (2020).
- [6] T. Liang, Q. Gibson, M. N. Ali, M. Liu, R. J. Cava, and N. P. Ong, *Nat. Mater.* **14**, 280 (2015).
- [7] K. S. Novoselov, A. K. Geim, S. V. Morozov, D. Jiang, M. I. Katsnelson, I. V. Grigorieva, S. V. Dubonos, and A. A. Firsov, *Nature (London)* **438**, 197 (2005).
- [8] S. V. Morozov, K. S. Novoselov, M. I. Katsnelson, F. Schedin, D. C. Elias, J. A. Jaszczak, and A. K. Geim, *Phys. Rev. Lett.* **100**, 016602 (2008).

- [9] C. Shekhar, A. K. Nayak, Y. Sun, M. Schmidt, M. Nicklas, I. Leermakers, U. Zeitler, Y. Skourski, J. Wosnitzer, Z. Liu, Y. Chen, W. Schnelle, H. Borrmann, Y. Grin, C. Felser, and B. Yan, *Nat. Phys.* **11**, 645 (2015).
- [10] C. P. Weber, *J. Appl. Phys.* **129**, 070901 (2021).
- [11] D. Neubauer, J. P. Carbotte, A. A. Nateprov, A. Löhle, M. Dressel, and A. V. Pronin, *Phys. Rev. B* **93**, 121202(R) (2016).
- [12] A. Akrap, M. Haki, S. Tchoumakov, I. Crassee, J. Kuba, M. O. Goerbig, C. C. Homes, O. Caha, J. Novák, F. Teppe, W. Desrat, S. Koohpayeh, L. Wu, N. P. Armitage, A. Nateprov, E. Arushanov, Q. D. Gibson, R. J. Cava, D. van der Marel, B. A. Piot *et al.*, *Phys. Rev. Lett.* **117**, 136401 (2016).
- [13] I. Crassee, E. Martino, C. C. Homes, O. Caha, J. Novák, P. Tückmantel, M. Haki, A. Nateprov, E. Arushanov, Q. D. Gibson, R. J. Cava, S. M. Koohpayeh, K. E. Arpino, T. M. McQueen, M. Orlita, and A. Akrap, *Phys. Rev. B* **97**, 125204 (2018).
- [14] M. Neupane, S.-Y. Xu, R. Sankar, N. Alidoust, G. Bian, C. Liu, I. Belopolski, T.-R. Chang, H.-T. Jeng, H. Lin, A. Bansil, F. Chou, and M. Z. Hasan, *Nat. Commun.* **5**, 3786 (2014).
- [15] Z.-G. Chen, C. Zhang, Y. Zou, E. Zhang, L. Yang, M. Hong, F. Xiu, and J. Zou, *Nano Lett.* **15**, 5830 (2015).
- [16] E. Zhang, Y. Liu, W. Wang, C. Zhang, P. Zhou, Z.-G. Chen, J. Zou, and F. Xiu, *ACS Nano* **9**, 8843 (2015).
- [17] A. Narayanan, M. D. Watson, S. F. Blake, N. Bruyant, L. Drigo, Y. L. Chen, D. Prabhakaran, B. Yan, C. Felser, T. Kong, P. C. Canfield, and A. I. Coldea, *Phys. Rev. Lett.* **114**, 117201 (2015).
- [18] J. Feng, Y. Pang, D. Wu, Z. Wang, H. Weng, J. Li, X. Dai, Z. Fang, Y. Shi, and L. Lu, *Phys. Rev. B* **92**, 081306(R) (2015).
- [19] H. Li, H. He, H.-Z. Lu, H. Zhang, H. Liu, R. Ma, Z. Fan, S.-Q. Shen, and J. Wang, *Nat. Commun.* **7**, 10301 (2016).
- [20] X. Yuan, P. Cheng, L. Zhang, C. Zhang, J. Wang, Y. Liu, Q. Sun, P. Zhou, D. W. Zhang, Z. Hu, X. Wan, H. Yan, Z. Li, and F. Xiu, *Nano Lett.* **17**, 2211 (2017).
- [21] T. Zhang, K. J. A. Ooi, W. Chen, L. K. Ang, and Y. Sin Ang, *Opt. Express* **27**, 38270 (2019).
- [22] B. Cheng, N. Kanda, T. N. Ikeda, T. Matsuda, P. Xia, T. Schumann, S. Stemmer, J. Itatani, N. P. Armitage, and R. Matsunaga, *Phys. Rev. Lett.* **124**, 117402 (2020).
- [23] Q. Wang, C.-Z. Li, S. Ge, J.-G. Li, W. Lu, J. Lai, X. Liu, J. Ma, D.-P. Yu, Z.-M. Liao, and D. Sun, *Nano Lett.* **17**, 834 (2017).
- [24] J. Liu, F. Xia, D. Xiao, F. J. García de Abajo, and D. Sun, *Nat. Mater.* **19**, 830 (2020).
- [25] C. P. Weber, E. Arushanov, B. S. Berggren, T. Hosseini, N. Kouklin, and A. Nateprov, *Appl. Phys. Lett.* **106**, 231904 (2015).
- [26] C. Zhu, F. Wang, Y. Meng, X. Yuan, F. Xiu, H. Luo, Y. Wang, J. Li, X. Lv, L. He, Y. Xu, J. Liu, C. Zhang, Y. Shi, R. Zhang, and S. Zhu, *Nat. Commun.* **8**, 14111 (2017).
- [27] W. Lu, S. Ge, X. Liu, H. Lu, C. Li, J. Lai, C. Zhao, Z. Liao, S. Jia, and D. Sun, *Phys. Rev. B* **95**, 024303 (2017).
- [28] G. Zhai, C. Ma, J. Xiang, J. Ye, T. Li, Y. Li, P. Sun, G. Chen, X. Wu, and X. Zhang, *Phys. Rev. B* **101**, 174310 (2020).
- [29] F. Sun, Q. Wu, Y. L. Wu, H. Zhao, C. J. Yi, Y. C. Tian, H. W. Liu, Y. G. Shi, H. Ding, X. Dai, P. Richard, and J. Zhao, *Phys. Rev. B* **95**, 235108 (2017).
- [30] W. Lu, J. Ling, F. Xiu, and D. Sun, *Phys. Rev. B* **98**, 104310 (2018).
- [31] F. Sun, M. Yang, M. W. Yang, Q. Wu, H. Zhao, X. Ye, Y. Shi, and J. Zhao, *Chin. Phys. Lett.* **35**, 116301 (2018).
- [32] W. Zhang, Y. Yang, P. Suo, W. Zhao, J. Guo, Q. Lu, X. Lin, Z. Jin, L. Wang, G. Chen, F. Xiu, W. Liu, C. Zhang, and G. Ma, *Appl. Phys. Lett.* **114**, 221102 (2019).
- [33] C. Bao, Q. Li, S. Xu, S. Zhou, X.-Y. Zeng, H. Zhong, Q. Gao, L. Luo, D. Sun, T.-L. Xia, and S. Zhou, *Nano Lett.* **22**, 1138 (2022).
- [34] S. Kovalev, R. M. A. Dantas, S. Germanskiy, J.-C. Deinert, B. Green, I. Ilyakov, N. Awari, M. Chen, M. Bawatna, J. Ling, F. Xiu, P. H. M. van Loosdrecht, P. Surówka, T. Oka, and Z. Wang, *Nat. Commun.* **11**, 2451 (2020).
- [35] C. Zhu, X. Yuan, F. Xiu, C. Zhang, Y. Xu, R. Zhang, Y. Shi, and F. Wang, *Appl. Phys. Lett.* **111**, 091101 (2017).
- [36] R. H. M. Groeneveld, R. Sprik, and A. Lagendijk, *Phys. Rev. B* **51**, 11433 (1995).
- [37] Y. M. Dai, J. Bowlan, H. Li, H. Miao, S. F. Wu, W. D. Kong, P. Richard, Y. G. Shi, S. A. Trugman, J.-X. Zhu, H. Ding, A. J. Taylor, D. A. Yarotski, and R. P. Prasankumar, *Phys. Rev. B* **92**, 161104(R) (2015).
- [38] Y. Ishida, H. Masuda, H. Sakai, S. Ishiwata, and S. Shin, *Phys. Rev. B* **93**, 100302(R) (2016).
- [39] Y.-K. Yang, F.-X. Xiu, F.-Q. Wang, J. Wang, and Y. Shi, *Chin. Phys. B* **28**, 107502 (2019).
- [40] A. Sharafeev, V. Gnezdilov, R. Sankar, F. C. Chou, and P. Lemmens, *Phys. Rev. B* **95**, 235148 (2017).
- [41] S. N. Gupta, D. V. S. Muthu, C. Shekhar, R. Sankar, C. Felser, and A. K. Sood, *Europhys. Lett.* **120**, 57003 (2017).
- [42] A. J. Frenzel, C. H. Lui, Y. C. Shin, J. Kong, and N. Gedik, *Phys. Rev. Lett.* **113**, 056602 (2014).
- [43] S.-F. Shi, T.-T. Tang, B. Zeng, L. Ju, Q. Zhou, A. Zettl, and F. Wang, *Nano Lett.* **14**, 1578 (2014).
- [44] See Supplemental Material at <http://link.aps.org/supplemental/10.1103/PhysRevB.106.155137> for details of calculated magnitude of photoconductivity with respect to elevated electron temperature, and fitting-momentum scattering time with respect to pump fluence, delay time, and temperature, which includes Refs. [42,43].
- [45] M. Tinkham, *Introduction to Superconductivity* (McGraw-Hill/Krieger, New York, 1975/1980).
- [46] P. Cheng, C. Zhang, Y. Liu, X. Yuan, F. Song, Q. Sun, P. Zhou, D. W. Zhang, and F. Xiu, *New J. Phys.* **18**, 083003 (2016).
- [47] M. Uchida, Y. Nakazawa, S. Nishihaya, K. Akiba, M. Kriener, Y. Kozuka, A. Miyake, Y. Taguchi, M. Tokunaga, N. Nagaosa, Y. Tokura, and M. Kawasaki, *Nat. Commun.* **8**, 2274 (2017).
- [48] M. Beck, M. Klammer, S. Lang, P. Leiderer, V. V. Kabanov, G. N. Gol'tsman, and J. Demsar, *Phys. Rev. Lett.* **107**, 177007 (2011).
- [49] D. Talbayev, K. S. Burch, E. E. M. Chia, S. A. Trugman, J.-X. Zhu, E. D. Bauer, J. A. Kennison, J. N. Mitchell, J. D. Thompson, J. L. Sarrao, and A. J. Taylor, *Phys. Rev. Lett.* **104**, 227002 (2010).
- [50] H. Chu, L. Zhao, A. de la Torre, T. Hogan, S. D. Wilson, and D. Hsieh, *Nat. Mater.* **16**, 200 (2017).
- [51] Y. H. Pei, Y. J. Zhang, Z. X. Wei, Y. X. Chen, K. Hu, Y. F. Yang, H. Q. Yuan, and J. Qi, *Phys. Rev. B* **103**, L180409 (2021).
- [52] J. Demsar, R. D. Averitt, K. H. Ahn, M. J. Graf, S. A. Trugman, V. V. Kabanov, J. L. Sarrao, and A. J. Taylor, *Phys. Rev. Lett.* **91**, 027401 (2003).

- [53] J. Demsar, V. K. Thorsmølle, J. L. Sarrao, and A. J. Taylor, *Phys. Rev. Lett.* **96**, 037401 (2006).
- [54] V. V. Kabanov, J. Demsar, and D. Mihailovic, *Phys. Rev. Lett.* **95**, 147002 (2005).
- [55] J. Zhang, J. Yong, I. Takeuchi, R. L. Greene, and R. D. Averitt, *Phys. Rev. B* **97**, 155119 (2018).
- [56] A. Rothwarf and B. N. Taylor, *Phys. Rev. Lett.* **19**, 27 (1967).
- [57] E. E. M. Chia, D. Talbayev, J.-X. Zhu, H. Q. Yuan, T. Park, J. D. Thompson, C. Panagopoulos, G. F. Chen, J. L. Luo, N. L. Wang, and A. J. Taylor, *Phys. Rev. Lett.* **104**, 027003 (2010).
- [58] S.-T. Guo, R. Sankar, Y.-Y. Chien, T.-R. Chang, H.-T. Jeng, G.-Y. Guo, F. C. Chou, and W.-L. Lee, *Sci. Rep.* **6**, 27487 (2016).
- [59] A. N. Afanasiev, A. A. Greshnov, and D. Svintsov, *Phys. Rev. B* **99**, 115202 (2019).
- [60] I. Gierz, J. C. Petersen, M. Mitrano, C. Cacho, I. C. E. Turcu, E. Springate, A. Stöhr, A. Köhler, U. Starke, and A. Cavalleri, *Nat. Mater.* **12**, 1119 (2013).
- [61] B. Zhao, P. Cheng, H. Pan, S. Zhang, B. Wang, G. Wang, F. Xiu, and F. Song, *Sci. Rep.* **6**, 22377 (2016).